

Unraveling the Catalytic Pathway of Metalloenzyme Farnesyltransferase through QM/MM Computation

Ming-Hsun Ho,[†] Marco De Vivo,^{†,‡} Matteo Dal Peraro,[§] and Michael L. Klein*,[†]

Center for Molecular Modeling and Department of Chemistry, University of Pennsylvania, 231 South 34th Street, Philadelphia, Pennsylvania 19104-6323, Department of Drug Discovery and Development, Italian Institute of Technology, Via Morego 30, I-16163 Genova, Italy, and Laboratory for Biomolecular Modeling, Institute of Bioengineering, School of Life Sciences, Ecole Polytechnique Fédérale de Lausanne, EPFL, CH-1015 Lausanne, Switzerland

Received November 4, 2008

Abstract: The protein farnesyltransferase (FTase) is a Zn²⁺-metalloenzyme that catalyzes the farnesylation reaction, i.e., the transfer of the 15-carbon atom farnesyl group from farnesyl diphosphate (FPP) to a specific cysteine of protein substrates. Oncogenic Ras proteins, which are among the FTase substrates, are observed in about 20–30% of human cancer cells. Thus, FTase represents a target for anticancer drug design. Herein, we present a classical force-field-based and quantum mechanics/molecular mechanics (QM/MM) computational study of the FTase reaction mechanism. Our findings offer a detailed picture of the FTase catalytic pathway, describing structural features and the energetics of its saddle points. A moderate dissociation of the diphosphate group from the FPP is observed during the nucleophilic attack of the zinc-bound thiolate. At the transition state, a resonance structure is observed, which indicates the formation of a metastable carbocation. However, no stable intermediate is found along the reaction pathway. Thus, the reaction occurs via an associative mechanism with dissociative character, in agreement with the mechanism proposed by Fierke et al. (*Biochemistry* **2000**, *39*, 2593–2602 and *Biochemistry* **2003**, *42*, 9741–9748). Moreover, a fluorine-substituted FPP analogue (CF₃-FPP) is used to investigate the inhibitory effect of fluorine, which in turn provides additional agreement with experimental data.

Introduction

The protein farnesyltransferase (FTase), a Zn²⁺-metalloenzyme, catalyzes the transfer of the 15-carbon farnesyl group from the farnesyl diphosphate (FPP) to acceptor proteins that contain the so-called “CaaX” motif at the C-terminus^{1–3} (where C is the cysteine residue that is farnesylated, a is generally an aliphatic amino acid, and X is the terminal residue, which can be alanine, cysteine, serine, methionine, or glutamine^{4–7}). FTase activity is crucial in signal trans-

duction pathways such as proliferation and apoptosis of cells.^{8,9} In fact, the Ras superfamily and small GTPases including Ras, Rho, and Rab are important examples of proteins that are activated by FTase function. Nowadays, FTase represents one of the promising targets for anticancer drug design,^{10,11} being involved in the activation of oncogene proteins such as mutated Ras, which are related to the development of ~20–30% of human cancers.^{12,13}

FTase is a heterodimer, which consists of a 48 kDa α subunit and a 46 kDa β subunit.^{3,14} Crystallographic and kinetic studies have suggested a two-step mechanism for substrates binding to FTase^{15–17} whereby, initially, FPP binds to the hydrophobic cavity in the β subunit, and then the CaaX peptide substrate binds to form a ternary complex FTase/FPP/CaaX. One Zn²⁺ ion is accommodated in the

* Corresponding author. E-mail: klein@lrsn.upenn.edu. Phone: 215-898-8571. Fax: 215-898-5425.

[†] University of Pennsylvania.

[‡] Italian Institute of Technology.

[§] Ecole Polytechnique Fédérale de Lausanne.

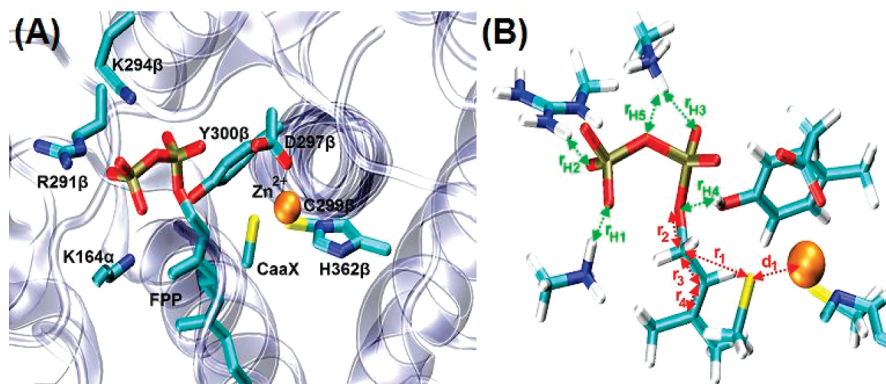


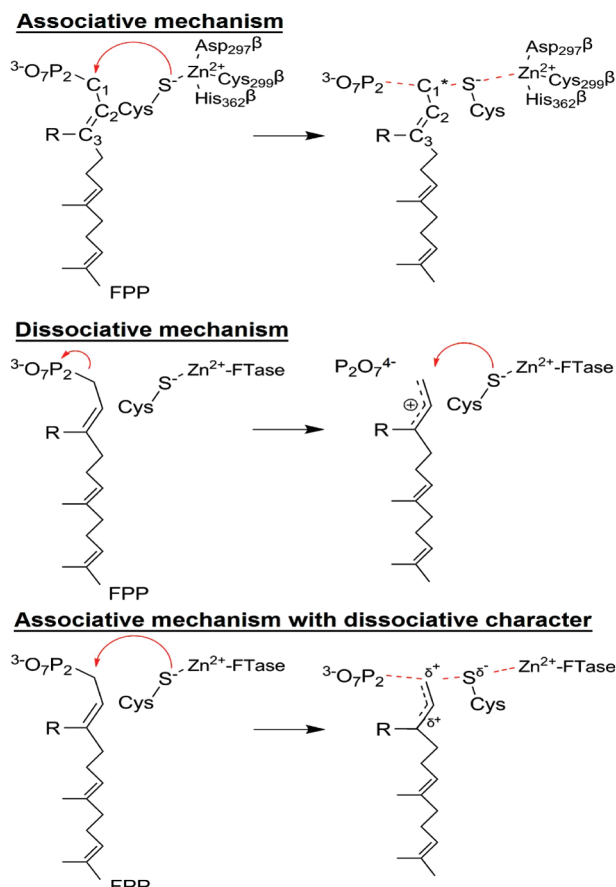
Figure 1. (A, Left Panel) A representative structure of the active site in the FTase/FPP/KCVIM ternary complex is shown. (B, Right Panel) the detailed conformation in the active site. The reaction coordinate is indicated by r_1 , which is the distance between sulfur anion S^- and C_1 carbon on FPP.

FTase catalytic site, and its presence is essential for efficient enzymatic activity.^{17,18} This metal ion is tetracoordinated to Asp 297 β , Cys 299 β , His 362 β , and the CaaX cysteine residue (Figure 1A). Recent experimental and computational results indicate that the CaaX cysteine is a thiolate in the bound state at physiological pH.^{19–21}

The FTase catalytic cycle involves two major steps: (1) the *physical step*, which consists of a conformational rearrangement needed to bring the FPP close to the nucleophilic thiolate in the ternary FTase/FPP/CaaX complex (the product of this step will be referred to as the *active form* hereafter), and (2) the *chemical step*, which is the transfer of the farnesyl group from the FPP to the thiolate.²² In particular, in the physical step the large separation between the reactive atoms C_1 of the FPP substrate and the sulfur atom of the thiolate must be spanned for the enzymatic reaction to occur. Indeed, the large value reported for this distance in the crystal structures^{5,23} ($r_1 = 7 \text{ \AA}$, Figure 1B) has led to the formulation of the so-called “distances paradox”²² for which two hypotheses have been suggested: (1) Rotation of the first two isoprenoid subunits of the FPP, so as to bring the reactive C_1 atom closer to the thiolate,^{17,22,24} or (2) dissociation of the thiolate from the Zn^{2+} ion and its subsequent approach to the FPP molecule.²⁵ Interestingly, a recent computational study has reported that the energy barrier for the rotation of the first two isoprene subunits of the FPP is lower than that of the dissociation of the thiolate from the Zn^{2+} ion coordination shell, thus favoring the first hypothesis.²⁶

Three distinct hypotheses have been proposed concerning the chemical step, all of which are based on various experimental findings² (Scheme 1). The first hypothesis suggests an $S_{N}1$ -like, “dissociative” mechanism, in which a stable carbocation is formed along the reaction pathway. Importantly, kinetic studies^{27–29} have shown a significant decrease of the reaction rate when different fluoromethyl FPP analogues are used as ligands. This would be caused by the destabilization of the carbocation intermediate, thus indicating an $S_{N}1$ -like mechanism for enzymatic activity. The second hypothesis suggests an “associative” $S_{N}2$ -like mechanism. This is supported by stereochemical studies that have shown inversion of configuration during farnesylation,³⁰ as well as by an observation of a α -secondary kinetic isotope

Scheme 1. Three Distinct Reaction Mechanisms for the Farnesylation Reaction Have Been Proposed^a



^a (Upper) Associative mechanism. (Middle) Dissociative mechanism. (Lower) Associative mechanism with dissociative character. R = CH_3 in the FTase/ CH_3 -FPP/CaaX system, while R = CF_3 in the FTase/ CF_3 -FPP/CaaX system.

effect that has shown a value near unity.³¹ Additional evidence for an associative $S_{N}2$ -like mechanism comes from a metal-substitution experiment: a 6-fold decrease in reaction rate has been measured when the zinc ion has been substituted by a cadmium ion in the FTase complex.²⁹ In fact, cadmium ions form stronger metal–ligand interactions with thiolate than zinc ions.³² As a result, this causes a decreased propensity for dissociation of the ligand (i.e., the

nucleophile) from the metal, which would lead to an associative interaction with FPP during the catalysis. Therefore, the decrease of the reaction rate in the Cd-FTase complex suggests an associative mechanism. Finally, a third mechanism has been proposed by Fierke et al. to explain the observation of both the nucleophilic and electrophilic character^{20,24,29,33} of the reaction under study. In the Fierke model, the enzymatic mechanism is proposed to have an associative transition state (TS), with a dissociative character, which suggests a hybrid of the first two mechanisms; the main characteristic of this pathway is a modest dissociation of the FPP diphosphate group during the early phase of the nucleophilic attack of the zinc-bound thiolate on the FPP molecule.

In view of the above scenario, a more detailed picture of the reaction mechanism and its transition state would improve our understanding of FTase enzymatic activity. Toward this aim, we focus on the chemical step of the catalytic cycle and present a computational study of the farnesylation mechanism. Our computations employ classical molecular dynamics (MD) and ab initio Car-Parrinello³⁴ (CP) QM/MM calculations. Based on the crystallographic structures, two different systems have been used in this work: a complex that includes the natural FPP substrate, and a second complex that includes the trifluoromethyl-sulfstituted FPP analogue, CF₃-FPP. Anticipating our results, we will see that, overall, our findings fit the experimental data rather well and thus provide additional insights into the nature of the farnesylation reaction mechanism and its inhibition by fluoromethyl-FPP analogues.

Methodology

Structural Models. A model of the FTase/FPP/CaaX ternary complex was generated based on the X-ray structure of Long et al.²² (PDB entry code: 1KZP, 2.1 Å resolution). This farnesylated product contains the dephosphorylated FPP molecule, the CaaX peptide formed by the KCVIM sequence of amino-acids, and the FTase protein. One FPP molecule was used to replace the dephosphorylated FPP. The FPP molecule was added to the structural model in order to restore the initial state of the ternary complex. In particular, the diphosphate group was rotated to have a linear configuration of O₁-C₁-S⁻ atoms (Figure 1B), while the isoprenoid chain matched the product form. The final model is consistent with the active form proposed by Long et al.²²

In order to study the electron-withdrawing effect of fluoromethyl-FPP analogues, we replaced the CH₃ group on the first isoprenoid group with a CF₃ group in the model system. This CF₃-FPP analogue represents the ligand used by Dolence et al. for kinetic experiments.²⁸

Molecular Dynamics. The FTase/FPP/CaaX ternary complex was immersed in a rectangular box of TIP3P waters (ca. 90 000 atoms in total). Classical MD was used to equilibrate the system and provide a suitable system for the subsequent QM/MM calculations. The AMBER force field (ff99)³⁵ was adopted for all standard residues, while RESP charges³⁶ were used for the Zn²⁺ ion, its ligands, and the FPP molecule. In order to simulate the FPP substrate, we

adopted the parameters from Cui et al. for the isoprenoid part of the FPP residue.³⁷ After the initial setup, a 10 ns MD trajectory was performed with the NAMD package.³⁸ The Zn²⁺ tetracoordination configuration was restrained. Full details of the set up procedure are reported in the Supporting Information. The system reached convergence after the first 4 ns of dynamics (see Supporting Information). The relevant distances in the complex and in particular the conformation of the FPP substrate did not significantly change during the multins time scale of the MD trajectory. The average distance separating the carbon C₁ and sulfur anion was 3.50 ± 0.20 Å. A representative snapshot, chosen from the equilibrated part of the MD trajectory, was used for the following QM/MM investigation.

QM/MM Dynamical Studies. The enzyme-catalyzed reaction was investigated using the Car-Parrinello (CP) MD version of the quantum mechanical (QM)/molecular mechanics (MM) method,³⁹ which has been proven to be an excellent tool in investigating the reactivity of solvated biological systems, including metalloenzymes.^{40–45} To this end, the model system was divided in two parts: (1) the active site region of the enzymatic complex, which was treated at the QM CP level with the DFT-BLYP functional,^{46,47} and (2) the remaining protein atoms and water, which were treated at the classical MD level with the AMBER force field. The use of the generally more reliable hybrid B3LYP⁴⁸ functional is unfortunately not possible for the present CP-MD simulations because of prohibitively heavy computational cost (about 2 orders of magnitude effort) associated with the use of B3LYP in CPMD.

In detail, the QM part of the system includes the Zn²⁺ ion, the side chains of the coordinated residues (namely, Asp297 β , Cys299 β , His362 β), the cysteine residue of the CaaX sequence, the diphosphate group and the first isoprene subunit of the FPP substrate, the side chains of the surrounding hydrogen donor residues (namely, Lys164 α , Arg291 β , Lys294 β and Tyr300 β), and one of the water molecules around the Zn²⁺ coordination shell. In total, 101 atoms were treated at the QM level (Figure 1B). A 25 Å × 20 Å × 20 Å supercell was used for the QM-CP system. The interaction between the valence electrons and the ionic cores are described with Troullier-Martins norm-conserving pseudo-potentials,⁴⁹ and a 70 Ry cutoff energy was applied. Simulations are carried out with a fictitious electron mass of 1000 au and a time step of 5 au (0.121 fs). The adiabaticity of the system was checked and assured (see Supporting Information for details). The interactions between the QM and MM regions are treated as in ref 39, and a rigorous treatment of the electrostatic interaction is implemented as in ref 50. The system was coupled with a Nosé-Hoover thermostat at 500 cm⁻¹ frequency to achieve constant temperature simulations.^{51,52}

The protocol of the QM/MM calculations includes an initial equilibration of the MD starting configuration. First, a short MD simulation was performed where the QM part is kept frozen, while the MM part is free to move for ca. 500 steps. Then, the whole system is allowed to move and gradually heat up to 300K in 1 ps. Finally, 1 ps of free QM/MM CP-MD was performed in order to equilibrate the

system, and provide a configuration to initiate the subsequent constrained QM/MM calculations. The enzymatic mechanism was investigated using a reaction coordinate (RC) defined as the distance between the two reactive atoms, namely the carbon C₁ on the FPP molecule and the S⁻ anion on the cysteine thiolate (Figure 1B). This RC was able to provide a fair description of the mechanism of nucleophilic substitution. An alternative choice of RC, defined as the difference between the length of the forming bond and that of the breaking bond, was also chosen to describe the reaction mechanism. Unfortunately, the latter RC failed to offer a reasonable picture of the reaction pathway (see Supporting Information for details).

So-called blue-moon ensemble simulations are performed for the model systems.⁵³ A constraint is applied at different values of the RC, whereas all other degrees of freedom are free to evolve. The catalytic reaction pathways are characterized in terms of (1) free energy profiles calculated using thermodynamic integration,⁵³ (2) variation of critical bond lengths, averaged over the last 1.5 ps of each constrained CP-MD QM/MM simulation; (3) variation of the electrostatic potential (D-RESP)⁵⁴ charges, calculated for all QM atoms during the QM/MM simulations, on the fly, and averaged over the last 1.5 ps of dynamics. Each step is simulated for at least 3 ps, or until the force on the constraint is equilibrated (i.e., the running averages over 1 ps windows varies less than 6%). The free energy profile is obtained by integration of the force profile. The error associated to each point of free energy profiles is calculated by propagating the error on forces at every step, using the propagation of error formula for linear functions. The present estimates of the free energies, based on these short ab initio CP-MD trajectories, should be considered rather approximate. Ideally, longer trajectories and several independent pathways should be investigated for a more accurate estimation of the enzymatic activation free energy, which unfortunately is not possible with currently available computational resources.

Results and Discussion

FPP Peptide Farnesylation. The free energy surface (FES) of the farnesylation reaction is computed using constrained dynamics, as explained in Methodology. Structural changes during the reaction mechanism are described in terms of averaged bond lengths. Twelve windows at different values along the reaction coordinate (RC) are considered in the interval [1.8, 4.0] Å. The RC is the internuclear distance between atoms C₁ and S⁻ (r_1 in Figure 1B), which represents the bond in formation. The distance between the atom C₁ and the oxygen O₁ of the diphosphate (PPi; r_2), namely the breaking bond, is instead free, together with all the remaining degrees of freedom.

The shape of the resulting FES of the FTase reaction is characterized by two minima, reactant (R) and product (P) states, separated by a single transition state (TS) (Figure 2). The local minimum in the R state is located around $r_1 = 4.0$ Å and $r_2 = 1.52$ Å. This structure is stable during a 2 ps free CP-MD QM/MM trajectory, which is consistent with the conformation produced by preparatory classical MD

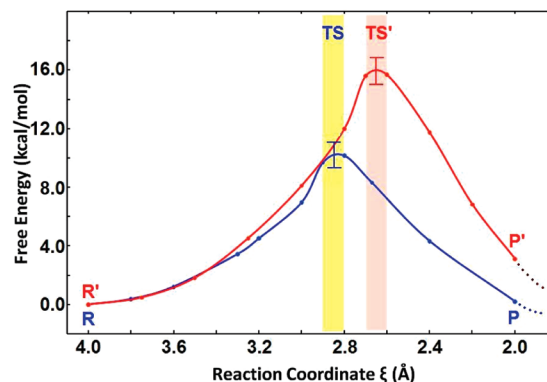


Figure 2. Calculated free energy surface (FES) of the farnesylation reaction. The FES obtained by using the FTase/CH₃-FPP/CaaX complex is shown in blue, while the one obtained by using the FTase/CF₃-FPP/CaaX complex is shown in red. The transition state regions along the two profiles are marked by colored rectangles.

(Figure 3). Simulations of the initial state R show a well-structured H-bond network that stabilizes the FPP binding conformation. Four amino acids are interacting with the substrate, acting as H-bond donors: Lys164 α , Arg291 β , Lys294 β , and Tyr300 β . This H-bond network is essential for the stabilization of the PPi and its electrostatic counterbalance.⁵⁵ Specifically, β -PPi H-bonds to Lys164 α ($r_{H1} = 1.51$ Å) and to Arg291 β ($r_{H2} = 2.65$ Å), while α -PPi H-bonds to Lys294 β ($r_{H3} = 1.73$ Å) (represented as black lines in Figure 3). Also, the O₁ atom H-bonds to the hydroxyl group on Tyr300 β ($r_{H4} = 2.26$ Å). This conformation of the active site in our simulations shows high similarity with the results previously reported from mutagenesis studies.²⁴ Interestingly, this H-bond network differs from that found in some X-ray structures and mutagenesis studies^{5,23,56} of the *inactive* form, where Lys164 α and Arg291 β interact with the α -PPi, while Lys294 β and Tyr300 β interact with β -PPi. The Zn²⁺ metal maintains its starting coordination with residues Asp297 β , Cys299 β , His362 β , and the cysteine thiolate from the CaaX motif. The average bond lengths of this tetracoordination compare well with the crystallographic ones: 2.08 Å (2.08 Å), 2.37 Å (2.21 Å), 2.14 Å (2.17 Å), and 2.35 Å (2.35 Å), respectively, with the crystallographic data shown in the parentheses.⁵

From R, we started to progressively decrease r_1 so as to approach the TS. Within [3.0, 4.0] Å interval no significant structural changes are observed, and the conformation of the farnesyl group, as well as the metal–ligand coordination, remains essentially unchanged (Figure 4). At $r_1 = 2.9$ Å, the distance between the thiolate and the Zn²⁺ metal ion becomes slightly longer ($d_1 = 2.35$ Å at $r_1 = 4$ Å versus 2.39 Å at $r_1 = 2.9$ Å). Importantly, this event precedes the nucleophilic attack of the thiolate on C₁, while r_2 increases from 1.52 Å (R state) to 1.57 Å. Also, at $r_1 = 2.9$ Å, resonance of bonds C₁–C₂ (r_3) and C₂–C₃ (r_4) starts to be evidenced by structural changes: the bond C₁–C₂ (r_3) decreases from 1.50 Å to 1.45 Å, while bond C₂–C₃ (r_4) becomes longer, from 1.35 Å to 1.37 Å, and thus suggest the approach of the TS region.

The TS region is located at 2.8 Å < r_1 < 2.9 Å, in which the averaged forces on the constraint are zero (Figure 2 and

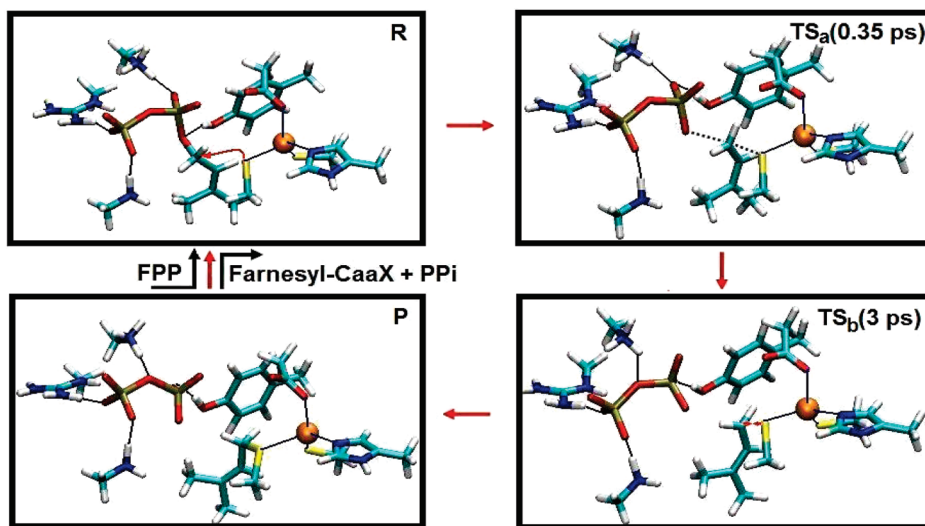


Figure 3. Selected snapshots taken from the reactive pathway of the farnesylation reaction. The metal–ligand coordination is indicated by blue lines. Hydrogen bonds are indicated by black lines. (R) Starting structure of the FTase/CH₃-FPP/CaaX complex. The Zn²⁺-coordinated thiolate plays a role as a nucleophilic group; (TS_a) selected structure at the transition state ($r_1 = 2.8 \text{ \AA}$) after 0.35 ps of dynamics. Here a modest dissociation of C–O bond (r_2), and a resonance of C₁–C₂ and C₂=C₃ bonds are observed. This points to a fairly dissociative character at the transition state; (TS_b) selected structure at the transition state ($r_1 = 2.8 \text{ \AA}$) after ~3 ps of dynamics. Now the diphosphate group dissociates completely from the farnesyl group; (P) the final product of the reaction is shown, where the new bond (C–S) is fully formed, indicating completion of the catalytic action.

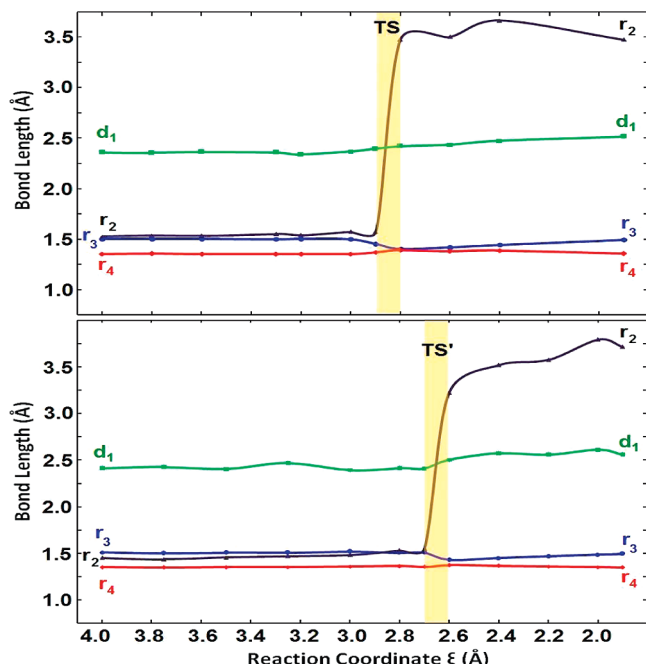


Figure 4. Selected average bond distances (label are indicated in Figure 1B) of the active site in the FTase/FPP/CaaX ternary complex along the investigated reaction pathways. (Upper Panel): FTase/CH₃-FPP/CaaX ternary complex. (Lower Panel): FTase/CF₃-FPP/CaaX ternary complex. The transition states are marked by colored rectangles.

Figure 3). Here, d_1 further elongates to 2.42 Å, indicating that the thiolate is dissociating from the zinc ion and is approaching C₁. At this point, r_2 spontaneously elongates (3.48 Å in TS versus 1.52 Å in R), leading to the definitive bond dissociation of r_2 and the subsequent carbocation formation. Then, the free PPi forms a stable hydrogen bond network with Lys164α, Arg291β, Lys294β, and Tyr300β.

Here, we observe a modification of the H-bond network around the PPi group, compared to that in R: Lys294β is now H-bonding to the linking O atom ($r_{H5} = 2.34 \text{ \AA}$) and Tyr300β is H-bonding to the α-PPi ($r_{H4} = 1.74 \text{ \AA}$), while Lys164α and Arg291β still H-bond to β-PPi ($r_{H1} = 1.47 \text{ \AA}$ and $r_{H2} = 1.88 \text{ \AA}$). Overall, all H-bonds become shorter when binding to the free PPi group, indicating a stronger electrostatic interaction. Also, r_3 decreases its length further, from 1.45 Å to 1.40 Å, and r_4 becomes slightly longer, from 1.37 Å to 1.39 Å. Although small in magnitude, the decreasing of r_3 together with the increasing of r_4 suggest resonance of the C₁–C₂ and C₂=C₃ bonds in the TS region, which indicates the likely formation of the carbocation on C₁. Nevertheless, we did not observe in the simulations a stable intermediate state in this region, indicating that a stable isolated carbocation is missing. Although we cannot definitely rule out the presence of such a stable intermediate, our findings suggest a reaction with an S_N2-like mechanism having a rather dissociative character, in agreement with the mechanism proposed by Fierke et al.^{24,29} Also, our results are further confirmed by a recent study of Lenevich et al., who have proposed a similar TS structure of a nonenzymatic reaction, based on computational calculations and kinetic isotope effect (KIE) studies of yeast FTase.⁵⁷ Finally, we point out that solvent water molecules do not seem to play an active role in the catalysis. In fact, there are few water molecules surrounding these two reactive atoms (C₁ and S[−]) at the TS region. Specifically, no water molecules are found within a 3 Å sphere centered on these two atoms, and only three within a 5 Å sphere, during catalysis.

After $r_1 = 2.8 \text{ \AA}$, the force on the constraint changes sign, indicating that the system is evolving toward the P state (Figure 3). The constraint is released after 3 ps of CP-MD QM/MM simulation at $r_1 = 2.8 \text{ \AA}$ and a stable product structure is formed. Here, $r_1 = 1.9 \text{ \AA}$, while $r_2 = 3.48 \text{ \AA}$.

The final structure agrees well with the crystallographic results;²² rmsd = 1.8 Å for the entire protein backbone and 0.7 Å for the active site residues. Moreover, the Zn²⁺ ion still maintains its coordination with Asp297 β , Cys299 β , and His 362 β , and distances compare well with the crystallographic data shown in square brackets:²² 2.03 [2.06] Å, 2.32 [2.27] Å, and 2.11 [2.18] Å, respectively. On the other hand, d_1 is now longer than in R (2.52 [2.66] Å in P²² versus 2.36 Å in R), indicating that the formation of r_1 weakens the Zn²⁺–S coordination, likely induced by a weaker charge interaction as discussed below in Charge Evolution during Catalysis.

CF₃-Substituted FPP Peptide Farnesylation. Fluorine substitutions on one methyl group of the alkyl chain of the FPP substrate have been studied to clarify the farnesylation reaction mechanism. The reaction rate drastically decreases when FPP analogues (CF₃-FPP) are used as substrates (from 770-fold²⁸ up to 3000-fold²⁹). This indicates that the trifluoromethyl group hinders the reaction and increases its energy barrier, suggesting a possible electrophilic mechanism. In order to investigate this hypothesis, we generated an FTase/CF₃-FPP/KCVIM complex within the present CP-MD QM/MM protocol. The setup employed for the QM system is identical to the wild-type study. Also, the procedure to define the FES remains the same.

With this analogue system, the FES shows two minima, reactant (R') and product (P') states, and one transition state (TS'). The R' state is stable around $r_1 \sim 4.0$ Å, as for the wild-type system (Figure 2). The catalytic site contains a large hydrophobic cavity that can easily accommodate the CF₃-FPP analogue; the diphosphate group forms a stable hydrogen bond network with Lys164 α , Lys294 β , and Tyr300 β . In details, Lys164 α H-bonds to β -PPi ($r_{\text{H}1} \sim 1.96$ Å), Lys294 β interacts both with α -PPi ($r_{\text{H}3} \sim 1.76$ Å) and β -PPi ($r_{\text{H}6} \sim 1.96$ Å), and Tyr300 β H-bonds to O₁ atom ($r_{\text{H}4} \sim 2.02$ Å). Here, we could not observe an H-bond between Arg291 β and PPi; this distance is larger than 3.5 Å. Overall, the Zn²⁺ tetracoordination is consistent with that in the wild-type system.

The structural conformation at the R' state is maintained from $r_1 = 4.0$ Å to 2.7 Å. The active site structure, including the farnesyl group and the metal–ligand coordination, does not change within this r_1 interval. The cysteine thiolate coordination to the Zn²⁺ ion is maintained as shown by d_1 , which does not change much (~2.41 Å in R'). Conversely, r_2 changes from 1.50 Å at $r_1 = 4.0$ Å to 1.61 Å at $r_1 = 2.7$ Å, reproducing the same trend as in the wild-type system, but with a larger amplitude. Unlike the resonance event we observed in the wild-type system, where r_3 and r_4 moderately change at $r_1 = 2.9$ Å, here r_3 and r_4 do not show significant changes (the differences between r_3 and r_4 is ~0.01 Å at $r_1 = 4.0$ Å and $r_1 = 2.7$ Å). This indicates that the fluorine substitutions on the methyl group hinder the resonance effect and destabilize the possible formation of a carbocation.

The TS' region is located at 2.6 Å < r_1 < 2.7 Å, where the averaged forces on the constraint are zero within the statistical error. Compared to the wild-type system, the TS' region is shifted by 0.2 Å. As for the wild-type, we could not observe a stable intermediate state. In terms of structural

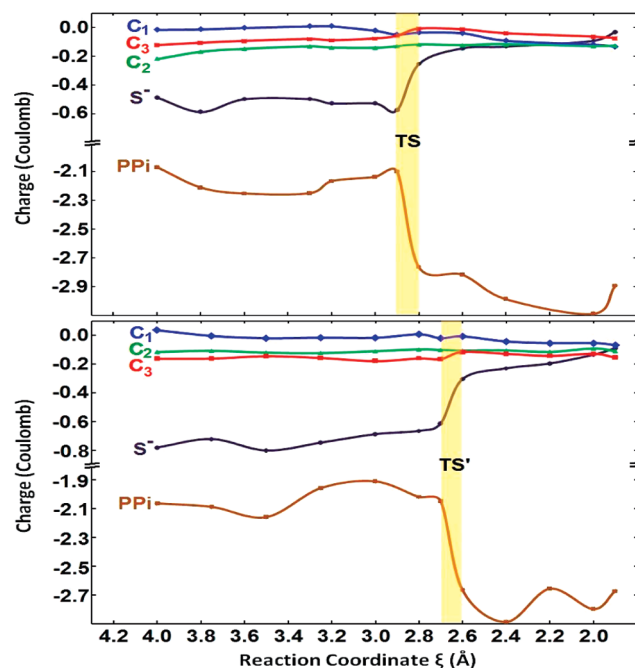


Figure 5. Profile of the ESP charge distribution on the active atoms and groups (labels of atoms/groups are indicated in Scheme 1) in the active site along the investigated reaction pathways. (Upper panel): FTase/CH₃-FPP/CaaX ternary complex; (Lower Panel): FTase/CF₃-FPP/CaaX ternary complex. The transition states are marked by colored rectangles.

changes, d_1 is 2.50 Å, showing that the nucleophile is actually approaching C₁. Concomitantly, the r_2 bond spontaneously breaks (3.41 Å, Figure 4). This clearly indicates the dissociation of the C–O bond. Also, r_3 decreases to 1.43 Å and r_4 elongates to 1.37 Å. This evidences a resonance structure that is similar to the wild-type case. At the same time, the dissociated PPi group forms H-bond interactions with Lys164 α , Lys294 β , and Tyr300 β . Now the $r_{\text{H}1} = 1.77$ Å, $r_{\text{H}3} = 1.87$ Å, $r_{\text{H}6} = 1.64$ Å, and $r_{\text{H}4} = 1.63$ Å. Only $r_{\text{H}3}$ is slightly longer than in R', whereas the rest of the values are shorter than in R'.

At $r_1 = 2.6$ Å, the force on the constraint changes sign, indicating that the system is falling into the P' well. The constraint is then released, and the system freely falls into the product well. The average bond length of C₁–S is 1.9 Å. In the P' region, the dissociated phosphate group continues to form a hydrogen bond network with the surrounding residues Lys164 α , Lys294 β , and Tyr300 β . Arg291 β does not play a role of H-bond donor, as previously observed. The conformation of the CF₃-FPP-farnesylated KCVIM peptide and the structure of the metal ion coordination match the crystallographic structure of the nonsubstituted product.²²

Charge Evolution during Catalysis. Both reaction pathways can be monitored through charge variations of relevant molecular moieties, as reported in Figure 5. The D-RESP atomic charge⁵⁴ was assigned to each QM atom, based on the electrostatic potential in the CP-MD QM/MM simulation computed on the fly.

In the wild-type system, at the initial state R, charge transfer effects occur at the metal–ligand coordination sphere: Zn²⁺ metal ion ($q = +0.16$ in units of electron charge) accepts electron density from Asp297 β , Cys299 β ,

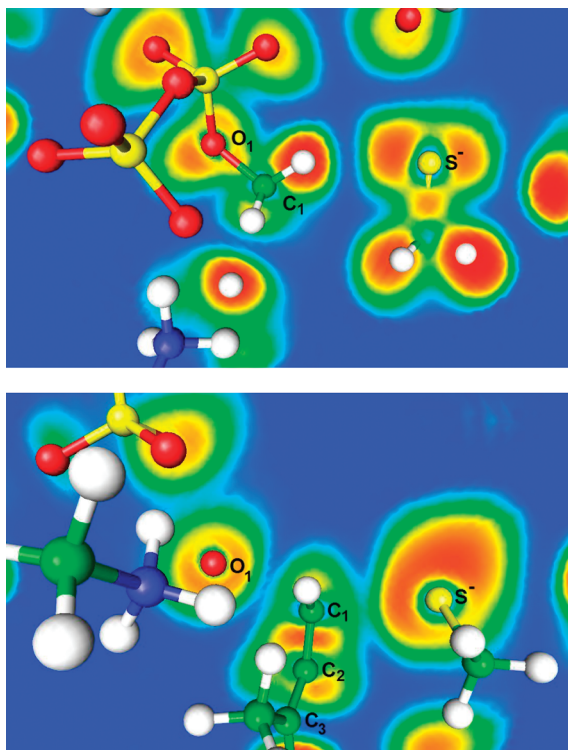


Figure 6. The calculated electron localization function (ELF) plot of the active site in the reagent state (upper) and the transition state (lower). The contour profiles are drawn through the plane of the O₁ and C₁ atoms the and S⁻ anion.

His 362 β , and cysteine thiolate ($q = -0.53$ on the S⁻ anion). Also, the C₁ atom is virtually neutral ($q = -0.01$) and both C₂ and C₃ atoms are negative ($q = -0.15$ and $q = -0.09$, respectively). A high electron density located on the PPi group reflects its negative charge ($q = -2.20$) and is stabilized by the H-bond interactions that involve the PPi group. At $r_1 = 2.9$ Å, the cysteine thiolate gains electron density ($q = -0.57$) due to its partial dissociation from the metal ion. This shows the nucleophilic character of the thiolate. Here, PPi does not dissociate yet and the local electron density remains the same. At the TS region, PPi spontaneously dissociates and gains electron density ($q = -2.76$). Meanwhile, the decrease of electron density on C₂=C₃ bond is concomitant with the neutralization of the charge of C₁ and C₃ atoms: this evidences a resonance structure formed by C₁, C₂, and C₃ atoms in TS, which is also supported by structural changes discussed earlier (i.e., change of r_3 and r_4 lengths). In particular, the resonance structure shows a partial positive charge transferred on these three atoms ($q = -0.24$ at R to -0.15 at TS). This finding supports a dissociative character with partial positive charge formed in the TS region. Moreover, a charge transfer occurs between the thiolate ($q = -0.25$) and the C₁ atom ($q = -0.03$), showing that the forming positive charge is shared between C₁ and S⁻ and therefore indicating that the thiolate is attacking the C₁ atom. The calculation of the electron localization function⁵⁸ (ELF) also shows that a covalent bond between the sulfur anion and the carbon atom C₁ (Figure 6) starts to form at the TS region. This explains the decrease of the negative charge on the nucleophile. The observation of the resonance of bond r_3 , r_4 , together with the calculation

of the atomic charge and ELF calculation, reveals that the reaction mechanism is either a pure associated or a dissociated mechanism. The structural and electronic property of the transition state in our QM/MM simulation suggests that a weak covalent bond forms between C₁ and S⁻. At the same time, the resonance of the group C₁, C₂, and C₃ stabilize the forming partial positive charge, which is due to the dissociation of the diphosphate group. Interestingly, this result is similar to several experimental findings that support a mechanism like the one described above.^{20,24,29,33} In P, the thiolate loses electron density while the r_1 progressively decreases, and the atomic charge on S⁻ anion becomes $q = -0.03$ at the final point. This indicates that the thiolate now is bound to C₁ and coordinated to the Zn²⁺ at the same time. Also, C₁ gains electron density from the thiolate and the charge becomes $q = -0.13$. Finally, C₂ and C₃ gain back electron density, although to a lesser extent compared to that in R ($q = -0.13$ and -0.07 , respectively).

The charge distribution along the reaction in the fluorinated system is virtually identical to that in the wild-type. In R', the electron density on C₁ and C₂ ($q = 0.00$ and -0.11 , respectively) is similar to that in the wild-type system. Also, C₃ gains electron density from the nearby trifluoromethyl group ($q = -0.16$). The charge distribution does not change when r_1 decreases from 4.0 Å to 2.7 Å. It is worth noting that upon reaching TS', the electron density on C₁, C₂, and C₃ does not change significantly ($q = -0.27$ to $q = -0.23$). This finding might be explained by the electrostatic effect of the CF₃-FPP. Finally, in the P' state, the farnesylated cysteine thiolate still binds to the zinc ion and the charge on the sulfur anion is $q = -0.08$, similar to the wild-type system. Therefore, the main difference between TS and TS' states is the charge distribution, where the C₁, C₂, and C₃ resonance group shows less positive charge in the fluorinated system. This possibly destabilizes the transition state and thereby induces the observed increase of the energy barrier.

Energetics of the Enzymatic Reactions. The free energy profile of different systems (FPP-KCVIM peptide and CF₃-substituted FPP-KCVIM peptide) are computed by thermodynamic integration of the constrained forces along the RC, as described the Methodology and plotted in Figure 2. The free energy barrier in the wild-type system is 10.8 ± 1.0 kcal/mol and 17.2 ± 1.0 kcal/mol in the CF₃-FPP system. Based on transition state theory, the reaction rate in the wild-type system is approximately 4 orders of magnitude faster than that in the fluorinated one. Given the uncertainty related to the calculated free energies and the fact that different CaaX motifs (CVLS²⁹ and CVIA²⁸) were adopted in the experimental measurement, this result agrees fairly well with experimental data,^{28,29} which report that the reaction rate for the CF₃-FPP system is slower than the wild-type by 3 to 4 orders of magnitude.

The experimental reaction rate is 0.017 s⁻¹ in an FPP-GCVLS peptide system²⁹ and is 0.0026 s⁻¹ in FPP-TKCVIF peptide system,⁵⁹ values that correspond to a barrier of 20.0 and 21.1 kcal/mol, respectively. These experimental values actually refer to the complete catalysis, the physical step (i.e., the conformational change of FPP) followed by the chemical step (i.e., the farnesylation reaction), while this study is

focused only on the latter. Thus, a direct quantitative comparison of experimental and theoretical enzymatic activity is difficult. Nevertheless, it is worth mentioning that a recent DFT study, which was carried out with a different procedure compared to the one applied herein, has reported that the cost of bringing the two reactive groups close to each other to overcome the physical step barrier is 10 kcal/mol.²⁶ If one assumes that the two steps (physical and chemical) are additive, then there seems to be good agreement between the computed and experimental barriers. The possibility that the barriers of the physical and chemical steps are additive is suggested by the lack of the “intermediate” state in the active reagents, as evidenced by several experimental findings such as spectroscopy studies and crystallographic data.^{2,22} This might indicate that, between the physical and chemical steps, the potential minimum is either missing (fully additive barriers) or relatively small. At this point, however, this rough comparison is somewhat speculative. Time-consuming accurate calculations on the physical step with the present methodology are currently in progress that will allow a correct comparison of the calculated enzymatic barrier with the experimental values.

The shape of the FES of the chemical step shows that the enzymatic reaction essentially follows an associative mechanism (i.e., no intermediate), where the TS is located between $r_1 = 2.8 \text{ \AA}$ and 2.9 \AA . We observe a significant resonance structure involving C₁, C₂, and C₃ atoms, together with a complete dissociation of the phosphate group at the TS region, which however does not lead to the formation of a stable intermediate. This can be explained by examining the structure, charge distribution, and the ELF plot at the TS region. As already mentioned in the previous section, a charge transfer occurred between the two reactive atoms, C₁ and S⁻. This indicates that the cysteine thiolate is interacting covalently with C₁ during the nucleophilic attack, in the TS. Therefore, though we observe dissociative characteristics along this reaction pathway, the overall chemical step should not be classified as a pure S_N1 mechanism.

The fluorinated system generally follows the same pattern, except from the fact that the TS' is at r_1 interval [2.6, 2.7] Å, where less resonance effects are observed. The free energy cost to bring r_1 from 4.0 Å to 2.8 Å is the same as that in the wild-type system, showing that the substitution of the methyl side chain on FPP does not introduce additional steric effects. Instead, the TS' state is destabilized due to the electron-withdrawing effect of the trifluoromethyl group and therefore results in a higher free energy barrier and a late TS event. This phenomenon is consistent with the observed structural information and charge transfer effect.

Conclusion

FTase has become a popular research subject since the discovery of the relation between its oncogenesis peptide substrates and the development of human cancers. To date, many potential FTase inhibitors have been extensively developed and showed encouraging preclinical results.⁶⁰ Some, such as tipifarnib and lonafarnib, were tested in human clinical trials.^{61–64} Moreover, recent studies point out that FTase inhibitors, originally considered only as anticancer

agents, show promising effects in treating malaria.^{65–68} As a result, FTase is currently a target in drug discovery and development.

Numerous crystallographic and kinetic studies have been performed for FTase, and different catalytic reaction pathways have been proposed. In this article, we have presented an investigation of the mechanism and energetics of the enzymatic reaction catalyzed by the FTase. In addition, the inhibitory effect of fluorinated substrate has been investigated, using a substrate analogue constituted by a CF₃-FPP.

The present simulations indicate the enzymatic reaction occurs via the so-called “associative mechanism with dissociative character”, in agreement with the proposed models based on experimental data.^{29,33,57} We observe a resonance structure in the TS region, which is concomitant with the formation of a metastable carbocation. Charge transfer effects along the reaction pathway confirm the resonance structure in the TS region. Nevertheless, no stable intermediate is found during the catalysis, suggesting a single-step mechanism. Inversion of configuration of the carbocation is also observed, in agreement with an S_N2-like mechanism. The dissociative character is explained by the fairly long length of the bond in breaking (3.5 Å) in the transition state, while the bond formation has a value of 2.8 Å.

The free energy for the chemical step of the catalysis is $10.8 \pm 1.0 \text{ kcal/mol}$. Interestingly, fluorine substitution of FPP (CF₃-FPP) increases the energy barrier to $17.2 \pm 1.0 \text{ kcal/mol}$, in agreement with the experimental measurements^{28,29} despite the fact that the reaction mechanism remains similar to that found with the FPP substrate. Charge transfer effects inducing destabilization of the carbocation formation in the CF₃-FPP reaction mechanism is the major reason for the increase of the barrier: the electron-withdrawing fluorine atoms hindered the reaction, leading to a higher energy for the transition state.

In summary, through the use of CP-MD QM/MM computations, we have proposed a picture of the FTase reaction mechanism and shed light on the inhibitory effect of fluorine substituents of the FPP substrate. The present description of the transition state conformations along the catalytic pathways might be helpful in the design of selective FTase inhibitors.

Acknowledgment. We thank the National Institutes of Health (NIH) for financial support and the Pittsburgh Supercomputer Center (PSC) for providing computational resources.

Supporting Information Available: Further details are given concerning the classical MD simulations, the QM/MM setup, the RESP charges used for the catalytic residues in the active site, the rmsd values of the enzyme along the trajectory, and snapshots illustrating the alternative pathways investigated. This material is available free of charge via the Internet at <http://pubs.acs.org>.

References

- (1) Zhang, F. L.; Casey, P. J. *Annu. Rev. Biochem.* **1996**, *65*, 241–269.

- (2) Sousa, S. F.; Fernandes, P. A.; Ramos, M. J. *J. Biol. Inorg. Chem.* **2005**, *10*, 3–10.
- (3) Lane, K. T.; Beese, L. S. *J. Lipid Res.* **2006**, *47*, 681–699.
- (4) Kato, K.; Cox, A. D.; Hisaka, M. M.; Graham, S. M.; Buss, J. E.; Der, C. J. *Proc. Natl. Acad. Sci. U.S.A.* **1992**, *89*, 6403–6407.
- (5) Long, S. B.; Hancock, P. J.; Kral, A. M.; Hellinga, H. W.; Beese, L. S. *Proc. Natl. Acad. Sci. U.S.A.* **2001**, *98*, 12948–12953.
- (6) Reiss, Y.; Stradley, S. J.; Giersch, L. M.; Brown, M. S.; Goldstein, J. L. *Proc. Natl. Acad. Sci. U.S.A.* **1991**, *88*, 732–736.
- (7) Hartman, H. L.; Hicks, K. A.; Fierke, C. A. *Biochemistry* **2005**, *44*, 15314–15324.
- (8) Vojtek, A. B.; Der, C. J. *J. Biol. Chem.* **1998**, *273*, 19925–19928.
- (9) Reuter, C. W. M.; Morgan, M. A.; Bergmann, L. *Blood* **2000**, *96*, 1655–1669.
- (10) Mazieres, J.; Pradines, A.; Favre, G. *Cancer Lett.* **2004**, *206*, 159–167.
- (11) Brunner, T. B.; Hahn, S. M.; Gupta, A. K.; Muschel, R. J.; McKenna, W. G.; Bernhard, E. J. *Cancer Res.* **2003**, *63*, 5656–5668.
- (12) Barbacid, M. *Annu. Rev. Biochem.* **1987**, *56*, 779–827.
- (13) Takai, Y.; Sasaki, T.; Matozaki, T. *Physiol. Rev.* **2001**, *81*, 153–208.
- (14) Reiss, Y.; Goldstein, J. L.; Seabra, M. C.; Casey, P. J.; Brown, M. S. *Cell* **1990**, *62*, 81–88.
- (15) Furfine, E. S.; Leban, J. J.; Landavazo, A.; Moomaw, J. F.; Casey, P. J. *Biochemistry* **1995**, *34*, 6857–6862.
- (16) Pompiliano, D. L.; Schaber, M. D.; Mosser, S. D.; Omer, C. A.; Shafer, J. A.; Gibbs, J. B. *Biochemistry* **1993**, *32*, 8341–8347.
- (17) Long, S. B.; Casey, P. J.; Beese, L. S. *Structure* **2000**, *8*, 209–222.
- (18) Reiss, Y.; Brown, M. S.; Goldstein, J. L. *J. Biol. Chem.* **1992**, *267*, 6403–6408.
- (19) Hightower, K. E.; Huang, C. C.; Casey, P. J.; Fierke, C. A. *Biochemistry* **1998**, *37*, 15555–15562.
- (20) Saderholm, M. J.; Hightower, K. E.; Fierke, C. A. *Biochemistry* **2000**, *39*, 12398–12405.
- (21) Sousa, S. F.; Fernandes, P. A.; Ramos, M. J. *J. Mol. Struct. (THEOCHEM)* **2005**, *729*, 125–129.
- (22) Long, S. B.; Casey, P. J.; Beese, L. S. *Nature (London)* **2002**, *419*, 645–650.
- (23) Reid, T. S.; Long, S. B.; Beese, L. S. *Biochemistry* **2004**, *43*, 6877–6884.
- (24) Pickett, J. S.; Bowers, K. E.; Hartman, H. L.; Fu, H. W.; Embry, A. C.; Casey, P. J.; Fierke, C. A. *Biochemistry* **2003**, *42*, 9741–9748.
- (25) Harris, C. M.; Derdowski, A. M.; Poulter, C. D. *Biochemistry* **2002**, *41*, 10554–10562.
- (26) Sousa, S. F.; Fernandes, P. A.; Ramos, M. J. *Proteins: Struct., Funct., Bioinf.* **2007**, *66*, 205–218.
- (27) Cassidy, P. B.; Poulter, C. D. *J. Am. Chem. Soc.* **1996**, *118*, 8761–8762.
- (28) Dolence, J. M.; Poulter, C. D. *Proc. Natl. Acad. Sci. U.S.A.* **1995**, *92*, 5008–5011.
- (29) Huang, C. C.; Hightower, K. E.; Fierke, C. A. *Biochemistry* **2000**, *39*, 2593–2602.
- (30) Mu, Y. Q.; Omer, C. A.; Gibbs, R. A. *J. Am. Chem. Soc.* **1996**, *118*, 1817–1823.
- (31) Weller, V. A.; Distefano, M. D. *J. Am. Chem. Soc.* **1998**, *120*, 7975–7976.
- (32) Pearson, R. G. *J. Am. Chem. Soc.* **1963**, *85*, 3533–3539.
- (33) Wu, Z.; Demma, M.; Strickland, C. L.; Radisky, E. S.; Poulter, C. D.; Le, H. V.; Windsor, W. T. *Biochemistry* **1999**, *38*, 11239–11249.
- (34) Car, R.; Parrinello, M. *Phys. Rev. Lett.* **1985**, *55*, 2471–2474.
- (35) Wang, J. M.; Cieplak, P.; Kollman, P. A. *J. Comput. Chem.* **2000**, *21*, 1049–1074.
- (36) Bayly, C. I.; Cieplak, P.; Cornell, W. D.; Kollman, P. A. *J. Phys. Chem.* **1993**, *97*, 10269–10280.
- (37) Cui, G.; Wang, B.; Merz, K. M. *Biochemistry* **2005**, *44*, 16513–16523.
- (38) Phillips, J. C.; Braun, R.; Wang, W.; Gumbart, J.; Tajkhorshid, E.; Villa, E.; Chipot, C.; Skeel, R. D.; Kale, L.; Schulter, K. *J. Comput. Chem.* **2005**, *26*, 1781–1802.
- (39) Laio, A.; VandeVondele, J.; Rothlisberger, U. *J. Chem. Phys.* **2002**, *116*, 6941–6947.
- (40) Dal Peraro, M.; Ruggerone, P.; Raugei, S.; Gervasi, F. L.; Carloni, P. *Curr. Opin. Struct. Biol.* **2007**, *17*, 149–156.
- (41) Dal Peraro, M.; Llarrull, L. I.; Rothlisberger, U.; Vila, A. J.; Carloni, P. *J. Am. Chem. Soc.* **2004**, *126*, 12661–12668.
- (42) De Vivo, M.; Ensing, B.; Klein, M. L. *J. Am. Chem. Soc.* **2005**, *127*, 11226–11227.
- (43) De Vivo, M.; Ensing, B.; Dal Peraro, M.; Gomez, G. A.; Christianson, D. W.; Klein, M. L. *J. Am. Chem. Soc.* **2007**, *129*, 387–394.
- (44) De Vivo, M.; Cavalli, A.; Carloni, P.; Recanatini, M. *Chem.—Eur. J.* **2007**, *13*, 8437–8444.
- (45) De Vivo, M.; Dal Peraro, M.; Klein, M. L. *J. Am. Chem. Soc.* **2008**, *130*, 10955–10962.
- (46) Becke, A. D. *Phys. Rev. A* **1988**, *38*, 3098–3100.
- (47) Lee, C. T.; Yang, W. T.; Parr, R. G. *Phys. Rev. B* **1988**, *37*, 785–789.
- (48) Amin, E. A.; Truhlar, D. G. *J. Chem. Theory Comput.* **2008**, *4*, 75–85.
- (49) Troullier, N.; Martins, J. L. *Phys. Rev. B* **1991**, *43*, 8861–8869.
- (50) Laio, A.; VandeVondele, J.; Rothlisberger, U. *J. Phys. Chem. B* **2002**, *106*, 7300–7307.
- (51) Nosé, S. *J. Chem. Phys.* **1984**, *81*, 511–519.
- (52) Hoover, W. G. *Phys. Rev. A* **1985**, *31*, 1695–1697.
- (53) Cicottti, G.; Ferrario, M.; Hynes, J. T.; Kapral, R. *Chem. Phys.* **1989**, *129*, 241–251.
- (54) Laio, A.; VandeVondele, J.; Rothlisberger, U. *J. Phys. Chem. B* **2002**, *106*, 7300–7307.
- (55) Bowers, K. E.; Fierke, C. A. *Biochemistry* **2004**, *43*, 5256–5265.
- (56) Strickland, C. L.; Windsor, W. T.; Syto, R.; Wang, L.; Bond, R.; Wu, Z.; Schwartz, J.; Le, H. V.; Beese, L. S.; Weber, P. C. *Biochemistry* **1998**, *37*, 16601–16611.

- (57) Lenevich, S.; Xu, J.; Hosokawa, A.; Cramer, C. J.; Distefano, M. D. *J. Am. Chem. Soc.* **2007**, *129*, 5796–5797.
- (58) Becke, A. D.; Edgecombe, K. E. *J. Chem. Phys.* **1990**, *92*, 5379–5403.
- (59) Pais, J. E.; Bowers, K. E.; Fierke, C. A. *J. Am. Chem. Soc.* **2006**, *128*, 15086–15087.
- (60) Bell, I. M. *J. Med. Chem.* **2004**, *47*, 1869–1878.
- (61) Doll, R. J.; Kirschmeier, P.; Bishop, W. R. *Curr. Opin. Drug Discovery Dev.* **2004**, *7*, 478–486.
- (62) Kurzrock, R.; Kantarjian, H. M.; Blascovich, M. A.; Bucher, C.; Verstovsek, S.; Wright, J. J.; Pilat, S. R.; Cortes, J. E.; Estey, E. H.; Giles, F. J.; Beran, M.; Sefti, S. M. *Clin. Cancer Res.* **2008**, *14*, 509–514.
- (63) Adjei, A. A.; Erlichman, C.; Davis, J. N.; Cutler, D. L.; Sloan, J. A.; Marks, R. S.; Hanson, L. J.; Svingen, P. A.; Atherton, P.; Bishop, W. R.; Kirschmeier, P.; Kaufmann, S. H. *Cancer Res.* **2000**, *60*, 1871–1877.
- (64) Ready, N. E.; Lipton, A.; Zhu, Y.; Statkevich, P.; Frank, E.; Curtis, D.; Bukowski, R. M. *Clin. Cancer Res.* **2007**, *13*, 576–583.
- (65) Gelb, M. H.; Hol, W. G. *J. Science* **2002**, *297*, 343–344.
- (66) Bulbul, V. J.; Rivas, K.; Verlinde, C. L.; Van Voorhis, W. C.; Gelb, M. H. *J. Med. Chem.* **2008**, *51*, 384–387.
- (67) Nallan, L.; Bauer, K. D.; Bendale, P.; Rivas, K.; Yokoyama, K.; Hornéy, C. P.; Pendyala, P. R.; Floyd, D.; Lombardo, L. J.; Williams, D. K.; Hamilton, A.; Sefti, S.; Windsor, W. T.; Weber, P. C.; Buckner, F. S.; Chakrabarti, D.; Gelb, M. H.; Van Voorhis, W. C. *J. Med. Chem.* **2005**, *48*, 3704–3713.
- (68) Olepu, S.; Suryadevara, P. K.; Rivas, K.; Yokoyama, K.; Verlinde, C.; Chakrabarti, D.; Van Voorhis, W. C.; Gelb, M. H. *Bioorg. Med. Chem. Lett.* **2008**, *18*, 494–497.

CT8004722